LUNFD6/(NFFL-7134) 1996

November 18, 1996

An investigation of the Parton Momentum Distribution in Diffractive Exchange using high p_T di-jets

Diploma work

Martin Karlsson[1]
Department of Physics
Lund University, Box 118
S-221 00 Lund, Sweden

[1] martin @ quark.lu.se

Abstract

A possible explanation to the occurrence of so-called diffractive events in electron-proton collisions at HERA is given through the introduction of an object called the pomeron. The pomeron is assumed to consist of gluons and quarks. In this report a variable describing the fraction of the total pomeron momentum carried by these so-called partons, the $x_{parton/IP}$ (parton/pomeron-x) has been studied.

The study was performed using data from computer simulations made with the RAPGAP Monte Carlo generator as well as experimental data collected with the H1 experiment in 1994. The description of the pomeron in the simulations is based on a pomeron structure function obtained from a fit to experimental data.

Our study of Monte Carlo simulated data shows that a determination of the $x_{parton/IP}$ is feasible i.e. the error of our measurement is expected to be satisfactorily low. The $x_{parton/IP}$ distributions from simulated and experimental data have been compared. Disagreements between these two distributions can be observed, indicating that the structure function used in the simulations does not give a correct description of the parton distribution. Alternatively, the experimental distribution might be better described by including the so-called 2-gluon exchange process, which was not done in our simulations.

Contents

1 Introduction

1.1 Elementary particles, “atoms”

Trying to explain what the world and the various objects around us are made of, the ancient Greek philosopher Democritos (about 460-380 b.c) stated that everything is built from tiny building-blocks, which he named atoms (atomos), meaning indivisible. Though his actual theory is not so good by today’s standards, the idea of the universe being built from some basic constituents is indeed now considered to be true. Particle physics is a field within physics developed during the 20th century aimed at finding and studying these constituents of the universe.

The *matter* which we are in contact with in our everyday life e.g. wood, plastic, water and air is made of *molecules* or combinations of molecules. The molecule is the smallest component of a material still having its characteristic (chemical) properties. Molecules are, roughly put, a bunch of *atoms* put together. The name atom has been kept through the years although it is a bit misleading. The atom is not indivisible. Experiments in the beginning of the 20th century first showed that atoms consist of an electrically positive *nucleus* surrounded by the so-called atomic *shells*, with most of the mass being concentrated to the nucleus. What we call shells are really point-like particles called *electrons* (e^-) that revolve around the nucleus. The electrons have small mass and carry a negative electric charge. The nucleus is built from neutral *neutrons*, n, and positive *protons*, p, giving it a net positive charge.

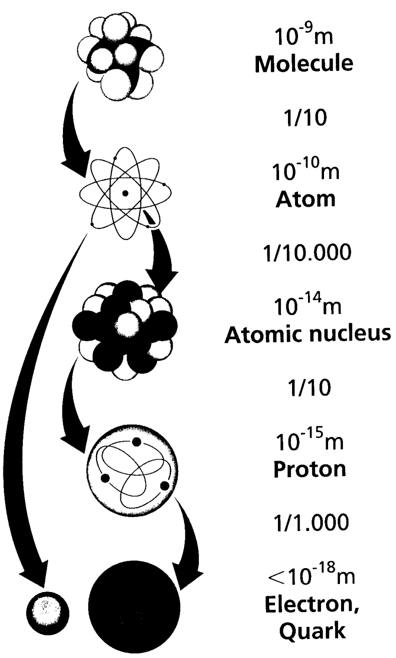

Fig 1.A : Order of size of the different components of matter .

Many of the elementary particles, e.g. the neutron, have been discovered through the study of cosmic radiation. The main instrument used to study particles today, however, is the particle accelerator, using a technology developed from the 1950’s and on. In accelerators, beams of particles are accelerated to high energies and made to collide with other particles. The particles resulting from this interaction are then detected, providing information on the collision mechanism.

Through the use of accelerators, one could see that the atomic nucleus had a measurable size (i.e. it was not point-like) and that it consisted of protons and neutrons as described above. The proton and neutron are also of measurable size, making it possible for them to have an inner structure. In the late 60’s, it was discovered that they each consist of three point-like particles that were named *quarks*.

The electron belongs to a group of particles called leptons. The different kinds of leptons known to exist today are by order of increasing mass: the electron (e^-), muon (μ^-) and tauon (τ^-), all point-like, having electric charge -1 (in units of the electron electric charge) and also the corresponding massless (or very small mass) neutrinos: the electron-neutrino (ν_e), μ-neutrino (ν_μ) and τ-neutrino (ν_τ). The neutrinos are electrically neutral. It is not believed that any other leptons exist.

$$
\begin{array}{c}
Q \\
\begin{array}{c} -1 \\ 0 \end{array}
\begin{pmatrix} e^- \\ \nu_e \end{pmatrix}
\begin{pmatrix} \mu^- \\ \nu_\mu \end{pmatrix}
\begin{pmatrix} \tau^- \\ \nu_\tau \end{pmatrix}
\end{array}
$$

Figure 1.B: The three lepton families.

Quarks exist in six different flavours (i.e. there are six different kind of quarks): up (u), down (d), strange (s), charm (c), beauty or bottom (b) and top (t). A quark with for example u-flavour is called a u-quark and so on. The u, s and t-quarks have charge (+)2/3, and the d, c and b-quarks have charge –1/3 (in units of electron charge). No quarks except those described above are believed to exist.

$$
\begin{array}{c}
Q \\
\begin{array}{c} +2/3 \\ -1/3 \end{array}
\begin{pmatrix} u \\ d \end{pmatrix}
\quad
\begin{pmatrix} c \\ s \end{pmatrix}
\quad
\begin{pmatrix} t \\ b \end{pmatrix}
\end{array}
$$

Figure 1.C: The three quark families.

Through certain reactions quarks can transform from one flavour into another. Quarks of large mass are very unstable. They decay into those more stable with smaller mass. The quarks most frequently existing in the universe are therefore the u and d-quark, the two least massive quarks. Triplets of these two make up the proton and neutron that together with the electron are the “cornerstones” of most universal matter. The real “atoms” in the true sense of the word “indivisible” and referring to them as the building-blocks of the universe are thus: the u-quark, the d-quark and the electron.

Particles consisting of a combination of quarks, like the proton and the neutron, are called hadrons. Hadrons are divided in two main groups, baryons like the proton and neutron, containing three quarks and mesons containing a quark and an antiquark. Hadrons have a total electric charge equal to the sum of the individual charges of its constituent quarks.

All particles have a “twin” particle with the same flavour and mass as itself. This twin is called the antiparticle of the particle. If a particle is charged, its antiparticle has the opposite charge. The concept of antiparticles was first suggested by Dirac and experimentally confirmed by the discovery of the antiparticle of the electron, the positive positron, denoted e^+. The antiparticle of a baryon consists of three antiquarks (e.g. the electrically negatively charged antiproton, $\overline{p}$) with the same flavours as those of its twin. The antiparticle of a meson, like its twin consists of a quark and an antiquark (but with the quark having the flavour of its twin antiquark and the antiquark having the flavour of its twin quark).

1.2 Interaction

The atomic nucleus and shell are held together by the attractive force between the negatively charged shell electrons and the positive core protons. This force of interaction between electrically charged particles is called the electromagnetic force. All the forces of nature can be seen as being mediated by “messenger” particles, travelling between the interacting particles, providing information of the interaction. The exchange of a messenger particle between two particles also means that momentum is transferred from one particle to the other. The mediator of the electromagnetic force is the photon, denoted γ. The photon is massless and travels with the speed of light. Electromagnetic interaction can therefore in principle take place over infinite distances. The theory describing the electromagnetic interaction is called quantum electrodynamics, QED.

Another force, similar to the electromagnetic, is the weak force. It is mediated by massive particles, the so-called gauge-bosons. The charged bosons W^+ and W^- mediate weak interaction involving the transition of electric charge and the neutral Z^0-boson mediates weak interaction not involving the transition of electric charge. Since the gauge-bosons are massive, they require a high amount of energy to be created and can (since a particle created with energy ΔE according to Heisenbergs uncertainty principle has a life-time limited to $\Delta t \sim h$[2]$/\Delta E$) travel only very short distances, which in principle makes it a point-like interaction. This interaction therefore has a low probability of occurrence, giving it the name “weak”.

Whenever the exchange of a photon is possible, Z^0-exchange is also possible. Electromagnetic and weak interaction are therefore viewed as one basic, electroweak interaction. At low energies weak interaction is less influential, but it is as important as the electromagnetic at high energies.

A big problem in particle physics was what force held the nucleus together. The protons of the nucleus electromagnetically repel each other. Still, the nucleus is a stable construction with protons and neutrons sticking together within a small radius. Also, according to the Pauli principle, no two different particles can have all so-called quantum numbers the same. The quantum numbers (e.g. electric charge, spin) describe the properties of a particle. It was however observed that the quarks of some different hadrons did have all quantum numbers the same. Furthermore, there was no explanation as to why no free quarks are ever found in nature. These problems were not totally solved and experimentally confirmed until in the 1980:s. To explain them one had to introduce a new force, stronger than the electromagnetic force, independent of electric charge and related to a new quantum number. This new force was called the strong force and it acts between particles carrying colour charge. There are three colours: red, green and blue, and three corresponding anticolours: antired, antigreen and antiblue. Hadrons are colourless, but the individual hadron quarks carry colour charge. The quark and antiquark of a meson must have charges colour, anticolour (or reverse) to make the meson colourless, they can for example be red and antired. The combination of three quark colours in a baryon must also be colourless, they can for

[2] The Planck constant $h = 6.626 \cdot 10^{-34}$ Js.

example be red, green and blue (added together giving white - colourless). Since no free coloured object has ever been detected, the rule of confinement was introduced, saying that coloured objects can exist only in colourless combinations, like the quarks do in hadrons.

The strong force is mediated by massless particles called gluons, denoted g. Gluons themselves carry colour charge, making it possible for them to interact with each other. Leptons have no colour charge and do not interact strongly. The theory describing strong interaction is called quantum chromo dynamics, QCD.

1.3 The model and experimental examination of the proton

The proton consists of two u-quarks and one d-quark, p = (uud). These are called the valence quarks of the proton. It also consists of gluons, mediating the strong force that holds the three quarks together. Through certain quantum fluctuations a gluon can temporarily split up into a quark-antiquark pair. The quarks created in this way are called sea quarks. Gluons can also due to self interaction split into pairs of gluons. The quarks and gluons of a proton are with a common name called the partons of the proton. The partons are free to move inside the proton (so called Fermi motion) and carry momentum.

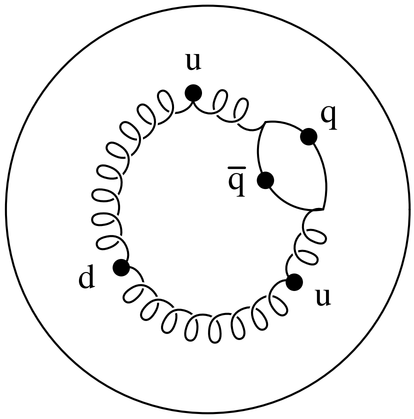

Figure 1.C: Simple picture of the proton inner structure.

To examine the inner structure of the proton, the point-like electrons may be used as "probes" by making them collide with the partons inside the proton. This is a kind of electron-proton (e-p) scattering. In view of experimental results and according to the theories of quantum mechanics, elementary particles do not only behave like what is expected from particles. They also have the properties of waves, propagating in space and time.

The wavelength, λ, of a periodic wave is the length of its period (see figure 1.D). The spatial resolution of e-p scattering is dependent on the electron wavelength, that is, the "probe particle" wavelength must be smaller than the object we are studying. This can be intuitively grasped by looking at figure 1.D. The electron wave of smaller wavelength, λ, has more "wiggles" inside the proton and is therefore more sensitive to an interaction with its contents, than the one with longer wavelength, λ'. Furthermore, the wavelength of a particle is inversely proportional to the particle momentum, p; $\lambda = h/p$. To achieve a small electron wavelength we hence want to give the electron a large momentum relative to the proton. The higher the particle energy, the larger the momentum. High electron and proton energies are therefore desirable. In Hamburg, the DESY collider HERA has

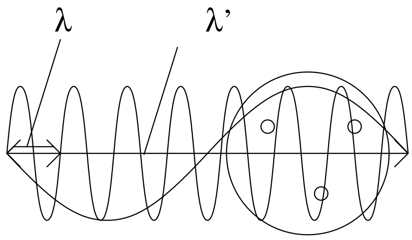

Figure 1.D: Intuitive picture of e-p scattering using different electron wavelengths ($\lambda < \lambda'$).

been in use since 1992. In this machine electrons of energy 30 GeV[3] and protons of 820 GeV collide, allowing studies of objects down to a size of 10^{-18} m.

To describe the interaction taking place in e-p scattering, the so-called proton structure function is used. The dimension-less structure function F_2 parmetrizes the parton content of the proton as the momentum distribution of the partons.

1.4 Thesis introduction

Usually, when a proton and electron collide the electron interacts with a coloured object (a gluon or quark) inside the proton. However, at HERA a class of events has been observed for which it seems that the electron interacts with a colourless object fluctuating from the proton. This object is, in some models describing these events, called *the pomeron* and the electron scatters against the constituents of this object, the pomeron partons. Scattering against the pomeron is described by using the *pomeron structure function* (analogous to the proton structure function).

The fraction of the total pomeron momenta carried by the scattered pomeron parton is denoted $x_{parton/IP}$. In this study, we will first determine with which accuracy it is possible to measure this variable. Then the $x_{parton/IP}$ distribution, retrieved both from experimental data and through computer simulation will be studied. This may tell us something about the pomeron structure and the properties of the pomeron partons. The computer simulation made is based on the pomeron model using a pomeron structure function that is a fit to experimental data. Comparing the simulated $x_{parton/IP}$ distribution with the experimental one, may hence give us an idea of how accurate our model of the pomeron is.

[3] 1 GeV = $1*1{,}60219*10^{-10}$ J

2 DESY, HERA and H1

In 1959 the DESY (Deutsches Elektronen Synchrotron) organisation was founded in Hamburg. Today, DESY has many different accelerators, the largest one (circumference 6336 m) is the electron-proton collider HERA. HERA consists of two so called storage rings, one for electrons of 30 GeV and one for protons of 820 GeV. Beams of electrons and protons circulate in these in opposite directions and collide at the interaction points of the two detectors ZEUS and H1.

2.1 The H1 detector

The H1 detector makes it possible to with unprecedented accuracy investigate the inner structure of proton. It is also among other things suitable for searching for hitherto unobserved particles.

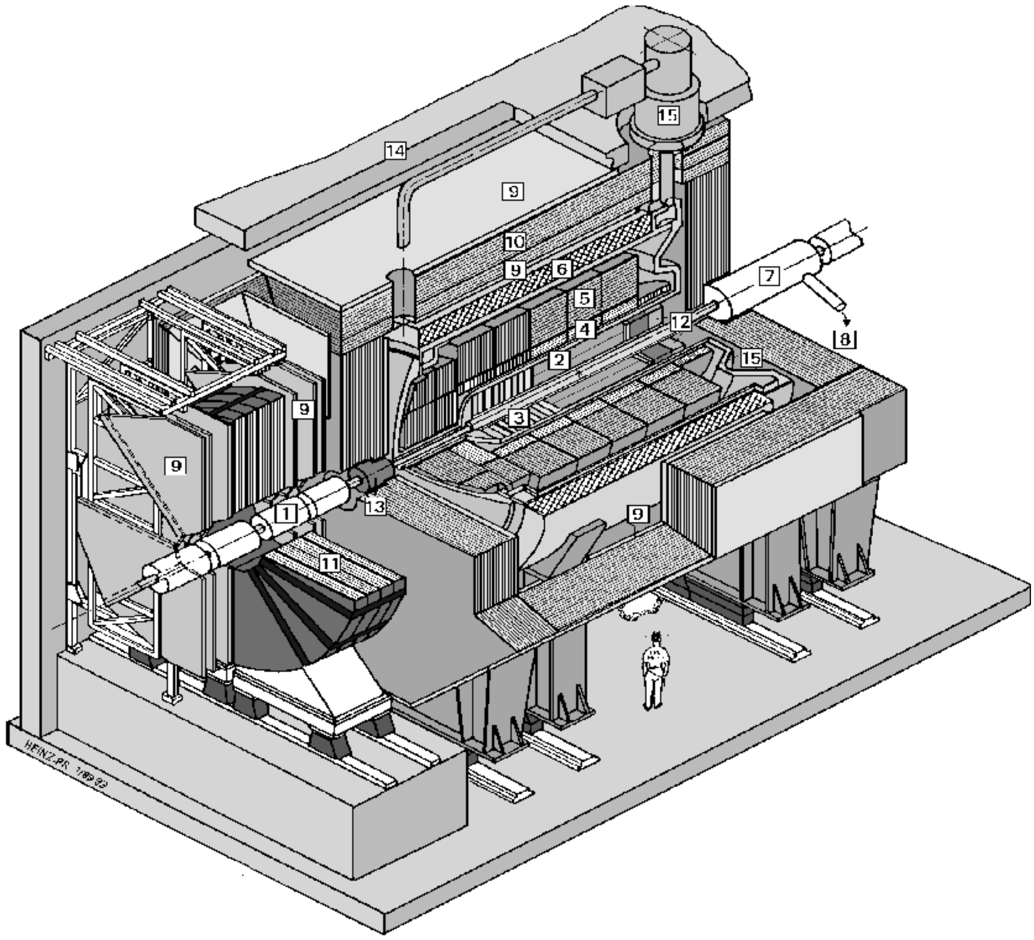

Figure 2.A : The H1 detector .

Since the HERA proton beam is more energetic than the electron beam, the particles emerging from the collision point will foremost travel in the proton direction of motion. Therefore, the H1 detector is asymmetric with denser instrumentation in this direction. The detector consists of the following parts, numbered according to figure 2.A.

The electrons and protons circulating in a high vacuum (1) *beam pipe* are directed to the interaction point by the beam magnets. Particles that do not leave the beam pipe can not be detected.

The (2) *Central tracking chambers* and (3) *Forward tracking and transition radiators* are made up of several wire chambers. A wire chamber consists of detection wires and wires generating an electric field, put inside a gas-filled container. Electrically charged particles that enter a wire chamber will interact with the gas atoms producing electron-ion pairs through ionisation. The electron-ion pairs are from the electric field acting on them given sufficient energy to reach the detection wires. This makes it possible to reconstruct a "track of ionisation" in the gas, made by the original charged particle. A magnetic field is applied from the outside to bend the trajectory of this particle. The bending is dependent on the particle velocity and therefore its momentum, and also its charge. The curvature of the track will hence provide information of these properties.

In the (4) *Electromagnetic calorimeter*, the energy of electrons, positrons and photons are absorbed whereas the hadrons deposit their energy in the (5) *Hadronic calorimeters*. This absorption happens through the production of so-called electromagnetic and hadronic showers respectively. That is, a particle entering the calorimeter medium interacts, primarily with its nuclei, giving secondary particles. These in turn interact, producing new particles and so on, resulting in a total shower of particles. In electromagnetic showers, the shower particles are electrons, positrons and photons. Hadronic showers are predominantly made up of hadrons. Higher mass hadrons decay into lower mass hadrons. The H1 calorimeter consists of a stack of lead and steel plates submerged in liquid argon. The lead plates are used in the electromagnetic and the steel plates in the hadronic calorimeter as absorption plates. Emerging from the plates, the showers enter the liquid argon and ionises it, creating so-called clusters of ionisation. The ionisation is collected on electronic pads producing a signal, proportional to the energy of the particles.

The (12) *Backward electromagnetic calorimeter (BEMC)* is used to detect the scattered electron of e-p scattering events. It is a lead scintillator sandwich, meaning that it consists of layers of scintillator material, material that when ionised by a charged particle emits visible light. This light then gives rise to a detectable pulse through so called photo multiplication.

The (13) *Plug calorimeter* is built for the study of particles travelling in the extreme forward direction with respect to the proton beam direction of motion. It can be used to detect the scattered proton, or proton remnant (the "broken up" proton rest) which keeps on travelling in the proton original direction of motion after the scattering has occurred.

In the (9) *Muon chambers*, muons are detected. Muons only interact weakly with nuclei and do not loose as much energy through radiation as for example electrons. They can therefore penetrate large quantities of iron almost without deflection and energy loss. This property of the muons is used to identify them. The *(10) Iron yoke* in this way functions as a muon "filter". The iron yoke is the outer shell of the detector and consists of a laminated structure of iron plates with streamer chambers inserted into the gaps. These chambers provide a rough measurement of the shower energy, which might not be fully contained in the calorimeter. In the detector forward direction, there is a separate muon spectrometer consisting of large tracking chambers before and after a (11) *Toroid Magnet*.

The iron yoke also acts as a return yoke for the H1 magnetic field, provided by the (6) *Superconducting coil* (cooled by liquid helium from the (8) *Helium cryogenics* system). The magnetic field acts on the particles in the central tracking chambers (as described above). The superconducting coil is situated on the "outside" of the calorimeters as not to disturb the particle detection, and its influence on the electron beam is compensated by the (7) *Compensating magnet*.

When the two particle beams are collided, different types of interaction will take place at a high rate. To sort out the interesting events and suppress the large so-called background of uninteresting ones, a trigger system is used. The triggers select events that satisfy certain specified conditions, and reject those that do not.

3 e-p scattering

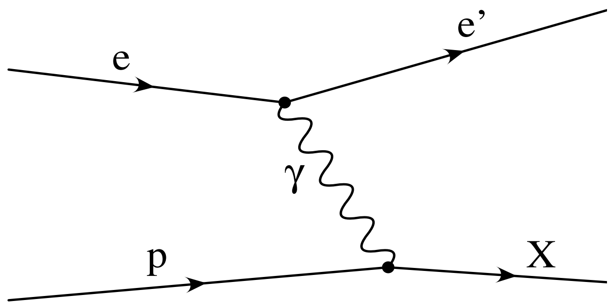

Figure 3.A: Generalised e-p scattering Feynman diagram.

Electron-proton scattering events are dominated by one-photon QED exchange between the proton and electron. As a calculational tool and visual aid for understanding interactions between elementary particle, so-called Feynman diagrams are used. The formalism of Feynman diagrams will not be described in any detail here, but we note that time "travels" from left to right in these diagrams. A generalised Feynman diagram of e-p scattering can be seen in figure 3.A, with letters denoting the particle types next to their respective Feynman representation.

The e-p scattering is called elastic when the proton after the scattering is intact, i.e. still "remains" a proton. This is written: $e^- + p \rightarrow e^- + p$ (X = p in fig. 3.A). The study of elastic e-p scattering led to the first measurements of the proton size.

When the proton breaks up, the scattering is called inelastic. This can be written: $e^- + p \rightarrow e^- + X$, where X denotes the so-called *hadronic system* which includes all particles produced by the interaction except the scattered electron. The kind of inelastic scattering in which the partons of the proton are "probed" (as mentioned in chapter 1.4) is called deep inelastic scattering, DIS.

If the partons of the proton are directly involved in the interaction, but the proton remains a proton after the scattering, it is called diffractive scattering, DS. Diffractive scattering is really also considered to be inelastic since the partons are probed, like in DIS. DIS and DS scattering will be discussed in more detail later on in this chapter (chapter 3.4 and 3.6 respectively). First, the concepts and formalism of e-p scattering will be looked into.

3.1 Coordinate system

In the formalism set up by the H1 experiment, e-p scattering events are described with respect to a coordinate system defined in the following way. The origin is placed in the collision point with the z-axis directed in the proton direction of motion. The x and y-axis are then chosen as to create a right-handed coordinate system. The polar

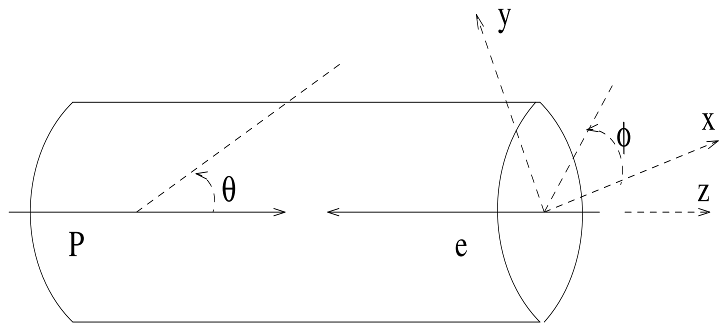

Figure 3.B: The H1 coordinate system.

angle, θ, is defined as measured from the positive z-axis. The azimuthal angle, ϕ, is defined in the xy-plane with the x-axis as reference.

3.2 Lorentz systems

The basic physical quantities which are important when studying elementary particles are energy and momentum and we thus introduce the particle four-vectors. If a particle has energy E and three-vector of momentum $\overline{p} = (p_x, p_y, p_z)$, its four-vector is written: $P = (E, \overline{p}) = (E, p_x, p_y, p_z)$.

Particles travelling at velocities close to the speed of light are affected by relativistic effects according to Einstein's special theory of relativity. A *Lorentz system* is a system of reference in which one has selected specific object to be at rest in the relativistic studies. The laboratory system is the Lorentz system defined as having the detector apparatus at rest. In DIS it is convenient to do studies in the system where proton and the exchanged photon balance each other, the so called γ-proton centre-of-mass system (CMS) also referred to as the hadronic CMS. It is defined as being the system where: $\overline{p}_\gamma + \overline{p} = 0$, with $\overline{p}_\gamma$ being the photon and $\overline{p}$ the proton momentum three-vector.

The invariant mass of a particle or group of particles is defined as the absolute of the sum of the particle four-vectors. That is, n particles having four-vectors $P_j = (E_j, \overline{p}_j)$, j = 1,2,…,n have a total invariant mass M, defined as:

$$M^2 = (\sum_{j=1}^{n} P_j)^2 = (P_1 + P_2 + \ldots + P_n)^2 = (E_1 + E_2 + \ldots + E_n)^2 - (\overline{p}_1 + \overline{p}_2 + \ldots + \overline{p}_n)^2$$

This mass has the same value in all Lorentz systems i.e. it is invariant with respect to the Lorentz system.

3.3 Kinematics

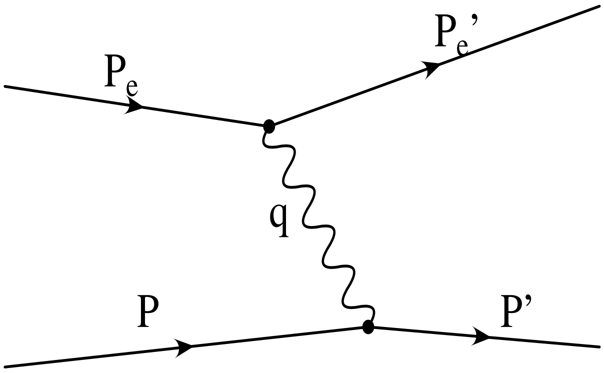

Figure 3.C: Illustrative picture of the e-p scattering four-vector denotation.

The different particle four-vectors of e-p scattering (see fig. 3.C) are denoted:

- beam electron four-vector: $P_e = (E_e, \bar{p}_e)$
- scattered electron four-vector: $P_e^{'} = (E^{'}_e, \bar{p}_e^{'})$
- beam proton four-vector: $P = (E, \bar{p})$
- the scattered proton four-vector: $P^{'} = (E^{'}, \bar{p}^{'})$
- exchanged photon four-vector: $q = (E_\gamma, \bar{p}_\gamma)$

Basic quantities, often used in the DIS formalism are:

- the square of the photon momentum transfer taken negative, Q^2, defined as: $Q^2 = -q^2 = (P_e - P_e^{'})^2$, and approximated by neglecting the electron mass ($m_e^2 \approx 0$): $Q^2 \approx 4 E_e E^{'}_e \cos^2 \theta_e / 2$, where $\theta_e = 180\text{-}\theta$ deg.

- the Bjoerken scaling variable defined as: $x = Q^2/(2\, P{\cdot}q)$

- Bjoerken y, the fraction of the electron energy transferred to the proton in the proton rest system, defined as: $y = (q \cdot P / P_e \cdot P)$, and approximated in the proton rest system to $y \approx E_\gamma / E_e$.

- the invariant mass of the total hadronic system W, defined as: $W^2 = (P + q)^2$, and approximated by neglecting the electron and proton masses ($m_p^2 \approx 0$ and $m_e^2 \approx 0$): $W^2 \approx Q^2\,(1/x-1)$.

The electron and proton rest masses can be safely neglected since they are small compared to the particle momenta.

Rapidity is a measurement of the polar angle θ, suitable for studies of e-p scattering, since it offers high resolution in the angular interval close to the proton direction of motion. If a particle has energy E and momentum p_z in the z-direction, its rapidity is defined as: $y = (1/2)\ln(E+p_z/E-p_z) = \tanh^{-1}(p_z/E)$. Neglecting masses, rapidity can be approximated with so-called pseudorapidity: $\eta = (1/2)\ln(p+p_z/p-p_z) = -\ln\tan\theta/2$

3.4 DIS processes

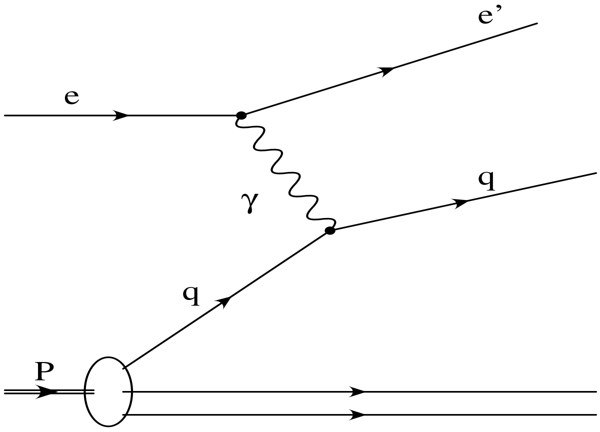

Figure 3.D: zeroth order DIS, QPM process Feynman diagram.

The simplest possible DIS process (Feynman diagram fig. 3.D) is when the electron scatters against a quark in the proton via exchange of a photon. In such a process the hadronic system consists of a scattered quark having four-momentum $P_p = xP$ and the broken up rest of the proton, the proton remnant. It is called a quark-parton model (QPM) process. The original beam proton, of course, is colourless, but the scattering process leads to two individual coloured parts, the quark and the proton remnant.

According to the rule of colour confinement no free coloured objects exist. Hence, the scattered quark and the proton remnant transform into hadrons (via the so-called fragmentation process which will be described in chapter 3.5) in the form of two collimated flows of particles, two *jets.* QPM events are therefore referred to as being *(1+1)-jet*, or *1-jet events* not counting the proton remnant jet. In this process, only QED interaction takes place. The Feynman diagram of the process does not contain any vertices representing QCD interaction and it can thus be classified as a *zeroth order QCD process*.

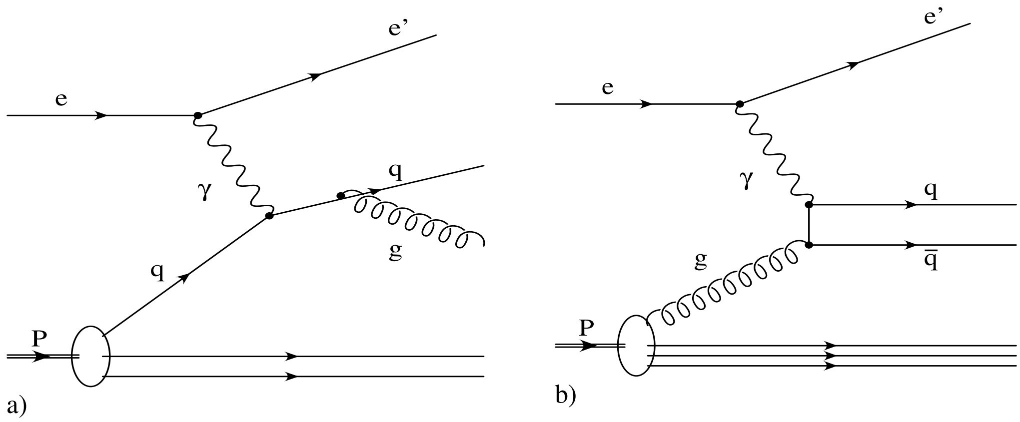

Figure 3.E: first order DIS processes, a) QCD-Compton and b) BGF

More complex DIS processes also exist. In a *QCD-Compton* process the electron (as in QPM) scatters against a quark in the proton via photon exchange, but the scattered quark in addtion emits a gluon. The probability for the quark to emit a gluon is determined by the strong coupling constant α_s. QCD interaction has taken place and the Feynman diagram of the process (fig. 3.E.a) contains a "three-parton" QCD vertex connecting the gluon and the quark before and after the emission. The QCD-Compton process is therefore classified as a *first order QCD* process.

A gluon in the proton can split up into a quark-antiquark pair. When the electron scatters against one of the quarks of such a pair it is called a boson-gluon fusion, BGF process. The BGF Feynman diagram (fig. 3.E.b) contains a three-parton QCD vertex (occurring with a probability determined by α_s) connecting the quark-antiquark pair and the gluon, making it too a first order QCD process.

The first order processes have two resulting partons and should therefore give rise to two jets in addition to the proton remnant jet. first order processes are therefore expected to be *(2+1)-jet* or *2-jet events.* First order processes are less probable to occur than zeroth order processes.

3.5 Parton showers, hadronisation and jets

The processes of e-p scattering are theoretically understood only to the point of the interaction on the basic level, the *hard interaction* as described above. The gluons and quarks produced by the hard interaction are called *hard partons*. To this description so-called phenomenological models must be added to account for remaining effects. The interacting partons are given the possibility to emit *soft* gluons both before and after the interaction with the photon has taken place, so-called initial and final state *parton showers*.

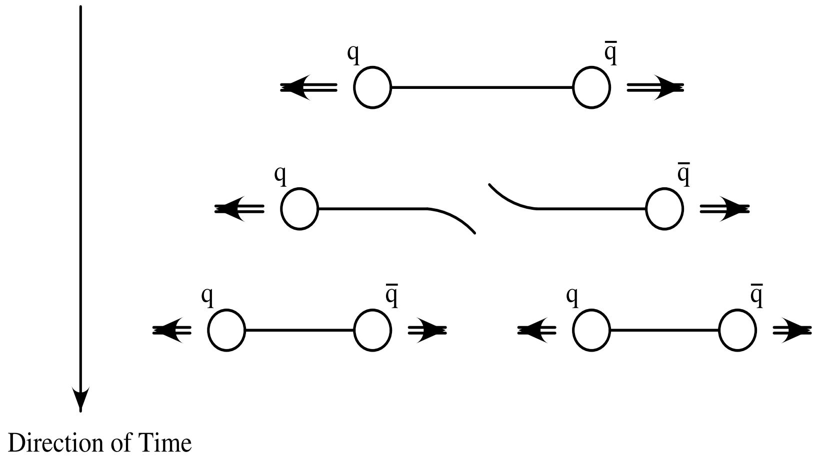

Figure 3.F: Schematic picture of the hadronisaton of a quark-antiquark pair according to the string model.

The strong force between particles is for large distances directly proportional to the distance between them (F(QCD)∝r). In the Lund string model this is described as something similar to two objects being attached to the ends of a rubber band. When the objects are pulled away from each other the band stretches, bursting if it is pulled hard enough. In this way the quark and antiquark of a colourless quark-antiquark pair can be regarded as being bound together by a so called colour string. The energy of the string increases as they move apart. If there is enough energy in the string to create new particles, it breaks, forming two or more colourless mesons. This is called the fragmentation or hadronisation process.

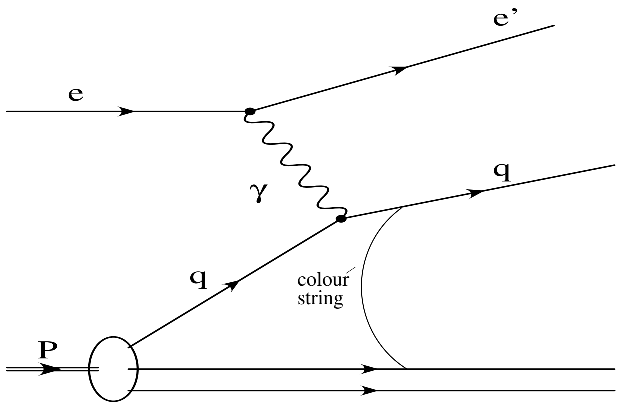

Figure 3.G: Illustrative picture of the colour string connections in a DIS QPM process.

In DIS, the exchanged photon transfers energy and momentum to the scattered parton. This makes the scattered parton move away from the other partons of the proton. It is then seen as being connected to them by a colour string. Hadronisation follows and the *final state particles* (hadrons) are created.

Provided that the energies of the hard partons are large enough, the final state particles will be emitted in a direction close to the hard parton direction of motion, thus giving rise to jets. On the other hand jets can not unambiguously be said to originate from the hard partons, since final state hadrons are created from the colour strings connecting the partons and also parton showers contribute to the creation of jets.

Particles are assigned to jets through the use of *jet algorithms*. There are many different algorithms offering different ways to pick out the jets. The input of a jet algorithm is often the four-vectors of the reconstructed final state particles. The algorithm then selects which four-vectors belong to jets and combines them to four-vectors representing the jets. These “jet four-vectors” are the output of a jet algorithm.

3.6 Diffractive pomeron events

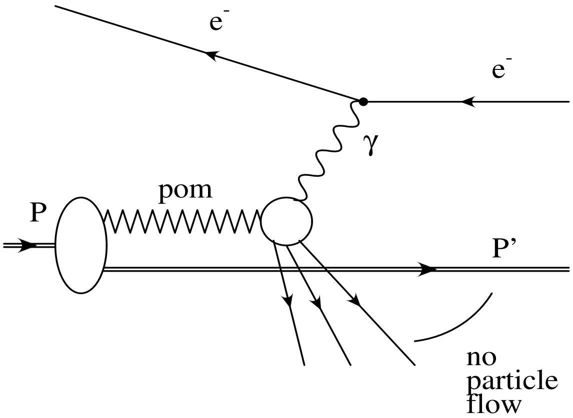

Figure 3.H: Illustrative picture of the basic structure of diffractive e-p scattering events.

In a standard DIS event, final state hadrons are distributed in the whole angular space between the proton and the hard partons, due to the hadronisation of the colour string stretched between them. At HERA, events have also been observed in which there are no hadrons in the angular region close to the beam pipe. The occurrence of such events were first noticed when studying rapidity distributions, and they are therefore called rapidity gap events. An explanation to the existence of such events is that the exchanged photon interacts with a colourless component, *the pomeron*, fluctuating the proton. The proton therefore remains colourless also after the scattering and continues its way down the beam pipe without breaking up, so called *diffractive scattering* (in this report denoted *DS*). The pomeron moves slightly away from the proton direction of motion. Since the proton remains colourless, there will be no colour strings connecting it and the rest of the system. Therefore, no hadronisation will take place close to the beam pipe.

The parton content of the pomeron and the momenta of the partons is (in analogy with the proton structure function) assumed to be parametrizable with the *pomeron structure function*. The structure function describing the parton content and momenta in diffractive scattering is denoted F_2^D . The pomeron is believed to consist of a combination of gluons and quarks. There are several hypothetical pomeron structure functions, based on different assumptions of what the pomeron consists of. They are thus either gluon or quark-based, meaning the pomeron content is assumed to be dominated by either gluons or quarks in the different models.

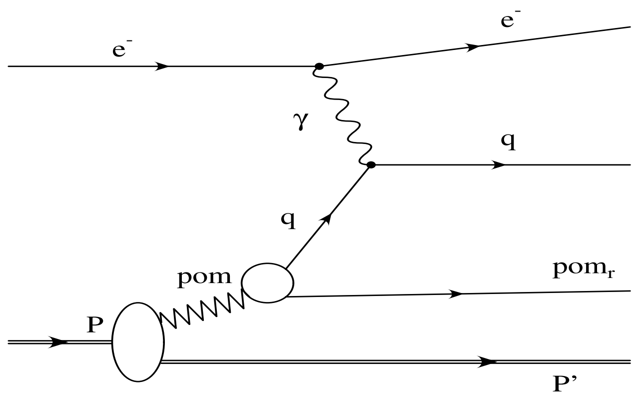

Figure 3.I: Feynman diagram of a DS zeroth order QPM process including the pomeron.

A model for a zeroth order pomeron process could in analogy with standard DIS ("replacing" the proton with the pomeron), be a QPM process in which the electron scatters against a quark in the pomeron (Feynman diagram in figure 3.I). The hard parton is like in DIS a quark. The structurally unaffected proton continues down the beam pipe. There would also be a pomeron remnant (regarded to be an antiquark for the pomeron to be colourless) as a result of the break-up of the pomeron.

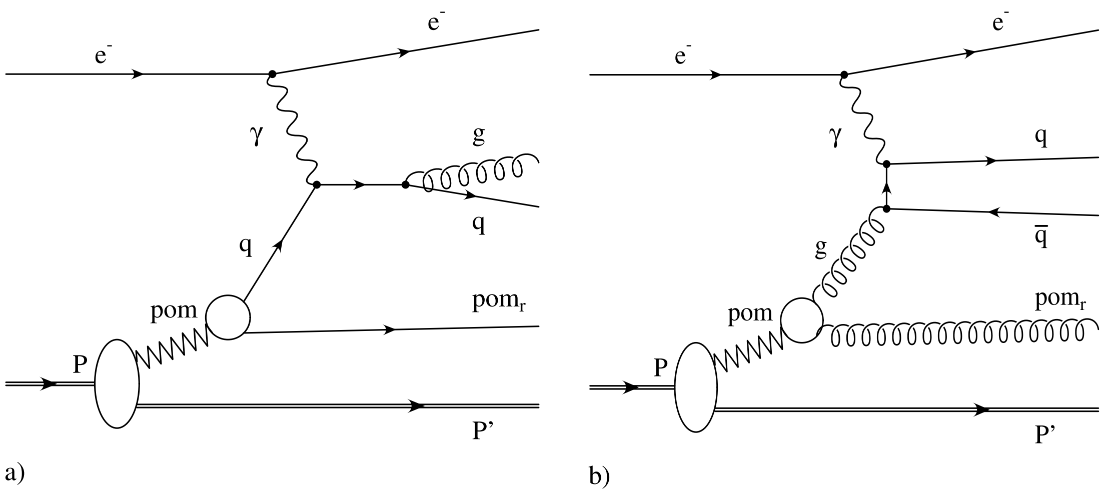

Figure 3.J: DS first order processes including the pomeron a) QCD-Compton and b) BGF

In correspondence with diffractive QPM, first order processes would be the diffractive QCD-Compton (Feynman diagram in fig. 3.J.a) and BGF (Feynman diagram in fig. 3.J.b) processes involving the pomeron. In analogy with DIS, the electron in the QCD-Compton process scatters against a quark in the pomeron producing a quark and a gluon. In the BGF process it scatters on one of the quarks of a quark-antiquark pair formed from a gluon fluctuating the pomeron. There is also, like for zeroth order DS, in both cases a pomeron remnant. (The pomeron remnant is seen as being an antiquark in the QCD-Compton process and a gluon in the BGF process.)

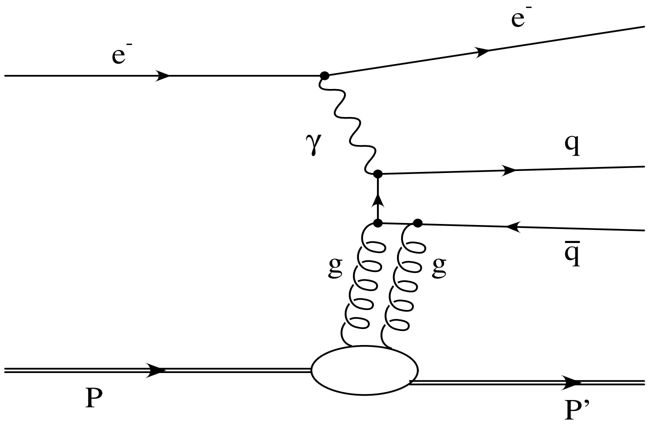

Figure 3.K: DS 2-gluon exchange process.

Another possible kind of DS process is the *2-gluon exchange* process (Feynman diagram fig. 3.K). The pomeron is here made of two gluons (and is therefore not the same "kind" of pomeron as the so-called soft pomeron involved in the processes described above), one splitting up into a quark-antiquark pair and the other "connecting" one of the pair quarks with the proton, making it a colourless object. In difference to the other DS processes, the 2-gluon exchange does not leave a pomeron remnant.

3.7 Generators and detector simulation

To get simulated results of e-p scattering, based on the current theories, so-called event *generators* are used. A generator is a computer program that calculates the probability for a certain process to occur and then produces the four-vectors of the particles resulting from the interaction of that process. For example, the RAPGAP generator generates rapidity gap events, based on the pomeron model. The calculation is done in steps: first the hard interaction, then the phenomenological models i.e. parton showers, colour strings and hadronisation. Results are available after each of these steps. The generator data is called *Monte Carlo* data, since Monte Carlo techniques are used in the calculations. Results from the hard interaction are referred to as the *parton level* and from the hadronic final state as results on the *hadron level*.

To be able to compare Monte Carlo data to experimental data, the effects of the detector must be taken into account. The detector itself affects the results in many ways. To impose detector effects on data directly produced by the event generator, a *detector simulation* is performed. This means that the Monte Carlo data is treated by a simulation program, containing information on how data is affected by the detector. The results are called *simulated detector level* results.

4 Methodology

In this chapter we will describe the derivations and the methods used in our study.

4.1 Kinematics of diffractive scattering: $\hat{s}$, M_x^2 and $x_{parton/IP}$

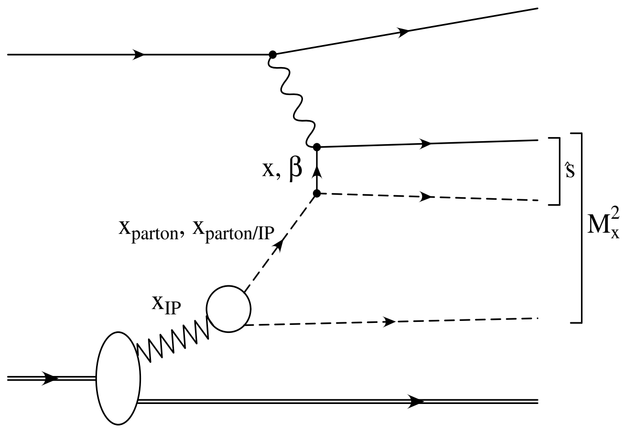

Figure 4.A: Illustrative picture of DS kinematic variables.

In diffractive pomeron events, M_x denotes the invariant mass of the hadronic system excluding the proton. On the parton level this corresponds to the total invariant mass of the hard partons and the pomeron remnant, *the diffractive system*. On hadron and detector level, M_x is calculated as the invariant mass of all final state particles detected outside the beam pipe. The invariant mass of the two hard partons in a first order DS event, *the hard subsystem*, is denoted $\hat{s}$. $\hat{s}$ is on the hadron and detector level calculated as the invariant mass of the two jets originating from the hard subsystem. ($\hat{s}$ can also be calculated from the jet rapidities, which has been tried in our study, but it gave inferior results and will therefore not be accounted for in this report.)

The variable Bjoerken-x ($x = Q^2/(2\,P\cdot q)$) is, as in DIS, the fraction of the proton momentum carried by the scattered parton interacting with the photon.
The "Bjoerken-x of the pomeron", β, is the fraction of the pomeron momentum carried by this parton. If $P_{IP} = (E_{IP}\,,\ \overline{p}_{IP})$ is the pomeron four-vector, we have

$$\beta = Q^2/(2\,P_{IP}\cdot q) \approx Q^2/(Q^2+M_x^2), \text{ since}$$
$$(P_{IP}+q)^2 = M_x^2, \text{ gives}$$
$$(2\,P_{IP}\cdot q) \approx Q^2+M_x^2, \text{ when } m_{IP}^2 << Q^2$$

x_{IP} (x-pomeron), the fraction of the proton momentum carried by the pomeron is given by

$$(x_{IP}P+q)^2 = M_x^2, \text{ so that}$$
$$x_{IP} \approx (Q^2+M_x^2)/2P\cdot q = (Q^2+M_x^2)x/Q^2, \text{ when } m_p^2 << Q^2$$

x_{parton} the fraction of the proton momentum carried by the parton scattered against in the pomeron is given by

$$(x_{parton}P+q)^2 = \hat{s}\text{, so that}$$
$$x_{parton} \approx (Q^2+\hat{s})/2P\cdot q = (Q^2+\hat{s})x/Q^2\text{, when } m_p^2 << Q^2$$

And, $x_{parton/IP}$, this partons fraction of the pomeron momentum by

$$(x_{parton/IP}\,P_{IP}+q)^2=\hat{s}\text{, so that}$$
$$x_{parton/IP} \approx (Q^2+\hat{s})/2\,P_{IP}\cdot q = (Q^2+\hat{s})/(Q^2+M_x^2),$$
$$\text{when } m_{IP}^2 << Q^2$$

If all of the pomeron momentum went into the pomeron remnant we would expect an $x_{parton/IP}=0$ and if there was no pomeron remnant, $x_{parton/IP}=1$.

In DS BGF processes specifically, this x is referred to as the x-gluon/pomeron, $x_{g/IP}$, since the parton is a gluon in this process. For QCD-Compton it is referred to as x-quark/pomeron, $x_{q/IP}$, since it is a quark there.

4.2 Jet selection and the CONE algorithm

A problem with some jet algorithms is that they are dependent on the Lorentz system in which they are applied. If we want to see the jets as carrying the properties of the hard partons, there is also a problem. Jets do (as mentioned in chapter 3.6) not totally reflect the hard parton properties, due to the effects of parton showers and fragmentation. Some particles included in the jets may therefore not satisfactorily reflect the hard parton properties. This lowers the jet resolution i.e. increases the difference between the jet properties and the hard parton properties. The jet resolution is dependent on the so-called cut-off variables included in the jet algorithm.

In this study, the CONE algorithm is used. In this jet algorithm, angular space is divided into equal sized cells in pseudo-rapidity, η and azimuthal angle, ϕ. The sum of the transverse energy $E_T = E\sin\theta$ deposited in each cell is calculated and cells having a total E_T above a certain value are considered as initiators of jets. Taking these initiators in order of decreasing E_T, the algorithm "checks" if a surrounding cone, having a beforehand chosen radius, $\Delta R = \sqrt{\Delta\phi+\Delta\eta}$, where $\Delta\phi$ and $\Delta\eta$ are the ranges in ϕ and η, has a total E_T greater than a cut-off parameter $E_{T(min)}$. If so, the cells define a jet. Instead of E_T, the almost equivalent quantity transverse momentum, $p_T = p\sin\theta \approx E_T$ (for high momentum, p), is often used, as

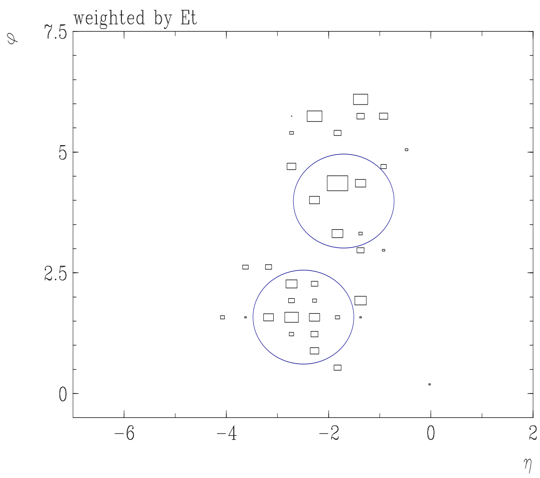

Figure 4.A: Energy flow in η−ϕ space

it is in this report.

The γ-parton CMS is the Lorentz system in which the total hard parton p_T is equal to zero. The resulting hard partons of a frist order DS event will thus in this system have equally large p_T in opposite directions. The pomeron remnant, though, like the pomeron has almost no p_T. If the CONE algorithm was applied in this system, the p_T cut would therefore exclude the particles originating from the pomeron remnant. First order processes are hence expected to become 2-jet events. The single hard parton in a zeroth order event will have a quite low p_T and such events should therefore be 0-jet events. For different reasons (e.g. the p_T of the hard parton jet is above the cut-off value or the pomeron remnant is counted as a jet by the jet algorithm), zeroth order events can sometimes be detected as 1 or even 2-jet events.

If we (like in this study) are interested in studying first order processes we look at 2-jet events. To exclude 2-jet events that are zeroth order processes, we can increase the p_T cut-off value in the jet algorithm. Increasing this value though also means cutting into first order events and thus decreasing the statistics.

Some of the particles from the pomeron remnant may be incorrectly included in the jets. Also, the proton remnant may sometimes escape the beam pipe, as is the case when so-called proton dissociation takes place. Particles originating from the proton remnant can therefore sometimes also be incorrectly included in the jets.

4.3 Reconstruction of particle four-vectors from experimental information

When studying simulated data and experimental data the most basic information is given in the form of electronic signals from the detector. From these signals we want to reconstruct four-vectors describing the properties of the final state particles as well as possible. By means of advanced reconstruction algorithms, information from each sub-detector is translated into a rudimentary four-vector “object”. The most important ones are the calorimeter objects called clusters and tracking chamber objects called tracks. The best i.e. most correctly reconstructed four-vector information of a detected particle is retrieved from a combination of both object properties.

The tracking chambers are closer to the beam pipe than the calorimeters. A bit of “dead” matter (matter not involved in actual detection) between the tracking chambers and calorimeter causes a loss of energy in the calorimeter. For low momentum tracks, the track information is therefore important. For high momentum tracks, a large amount of energy will go into the calorimeter. The track properties will not add any information (since the track “bending” is small), but the energy lost “on the way” to the calorimeter should still be accounted for.

Considering this, we will in our study take a low momentum track, p<350 MeV, as it is. If a track has large momentum, p>350 MeV, it is rescaled to p=350 MeV, and then used only to account for energy losses before the calorimeter. Tracks are then combined with clusters, creating so-called combined objects. Using combined objects much improved our results compared to only using clusters in the reconstruction.

5 Analysis

In this chapter we will describe the conditions and assumptions under which the study has been made. Then the results of the study will be shown and commented on.

Our final aim is to study the $x_{parton/IP}$ distribution for diffractive events from experimental data. This distribution provides information about the pomeron parton content and in the prolongation also the pomeron structure function. To determine the relevance of the results from experimental data, we first compare Monte Carlo data on the detector and hadron level. In this way we can estimate how large the distortions (smearing) due to detector effects are. Then we compare simulated and experimental data.

A file containing Monte Carlo events generated by the RAPGAP 2.1 generator and processed with the detector simulation program H1SIM was used. This version of RAPGAP does *not* include the 2-gluon exchange process. The experimental data used was H1 data from 1994. The analysis was made using the H1TOX analysis package. It provides the standard variables of e-p scattering in the form of blocks, each block containing a number of logically connected quantities. For each event the quantity values were calculated from data and stored in a so-called n-tuple. Plots were then extracted from the n-tuple using the PAW analysis workstation program.

5.1 The pomeron structure function

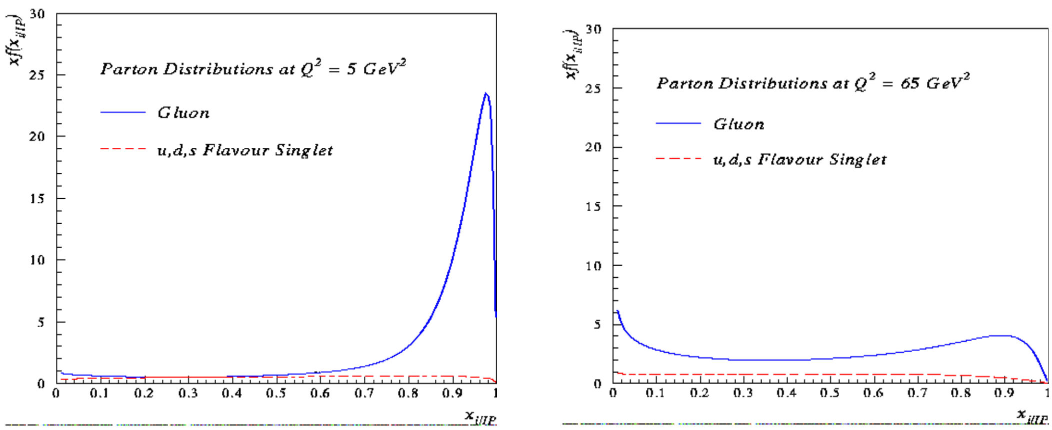

a) b)

Figure 5.A: The pomeron gluon and quark distributions at a) low energy, $Q^2 = 5\ (\mathrm{GeV})^2$ and b) high energy, $Q^2 = 65\ (\mathrm{GeV})^2$

The pomeron structure function used in this study is called the *singular gluon and quark* structure function. It is a fit to F_2^D data from inclusive measurements, which provide a description of the parton content in diffractive events. The pomeron is assumed to consist of both gluons and quarks. At a starting scale of $Q^2 = 4\ (\mathrm{GeV})^2$

the gluon distribution is peaked at large values of $x_{g/IP}$ and the quark distribution is flat in (i.e. independent of) $x_{q/IP}$. The quark contributions are small compared to the gluon contributions. Increasing Q^2, the gluon contribution still dominates and has the characteristic behaviour of increasing at low $x_{g/IP}$ and depleting at high $x_{g/IP}$.

For the 2-gluon exchange process, not included in the simulations of this study, we would expect a gluon distribution similar to a δ-function peaked at 1. This is expected since there is no pomeron remnant and thus $x_{parton/IP} = x_{g/IP} \approx 1$.

5.2 Choice of Lorentz system

Our studies are made in the hadronic (γ-proton) CMS. To "get to" this system from the laboratory system, we need to make a boost. This boost is determined by the kinematics reconstructed from the scattered electron. The errors of this reconstruction will therefore affect the boost and the reconstructed hadronic CMS will not be completely correctly defined.

The ideal Lorentz system for us to use would be the γ-parton CMS since it is the system were the total hard parton p_T is equal to zero. Boosting to this system requires an *a priori* knowledge of the properties of the pomeron parton defining it, which we do not have. The hadronic CMS is a natural frame for our analysis, since the total p_T of the hadronic final state particles is equal to zero in this system. It is preferred for the p_T based CONE algorithm, since the total hard parton p_T is close to zero. Thus, the single hard parton of a zeroth order event will have almost no p_T. In a first order event the two hard partons will have almost equal and oppositely directed p_T.

5.3 Data selection

For our results to have meaning we must disregard, cut away events that are not within a well defined kinematical region. Also cuts must be made to keep out events for which detector limitations makes the reconstruction unreliable.

In this analysis, the scattered electron is detected by the BEMC. Located in front of the BEMC is the Backward proportional chamber, BPC. Together with the vertex position reconstructed from tracks from the central tracker, the BPC provides the angular measurement of the electron whereas its energy is measured by the BEMC. The cuts we make on BEMC and BPC data, and the reconstructed electron kinematics are:

• The BEMC cluster must have energy weighted radius that is less then 5 cm, defining lateral spread and energy deposited in the BEMC.

• The distance between BPC tracks and BEMC clusters has to be less then 5 cm.

• The cuts on the x- and y-coordinates are $|x|<16$ cm and $|y|<16$ cm, the "box cut" and $|x+y|<18$ cm, "inner radius cut", defining the small angular acceptance of the BEMC.

• The reconstructed electron polar angle is cut at $\theta_e<3.019$ rad, to ensure that the scattered electron is well contained in the BEMC.

• Events must have reconstructed electron energy, $E_e^{'}>11$ GeV, to remove the background events in which the true electron escapes detection and a cluster (e.g. created by a photon, radiated by the electron through a bremsstrahlung process) is misidentified by the BEMC as being an electron.

• To avoid events in which there are large electron bremstrahlung effects, the difference between energy and longitudinal momentum for all objects (including the scattered electron), $\Sigma(E-p_z)$, must be within the range $40<\Sigma(E-p_z)<70$.

• For the y of the reconstructed electron we cut off events where y>0.05 to get an adequate resolution in this variable.

The point in the tracking chambers from which the particles from a collision seem to originate along the z-axis, is defined as the event z-vertex. On this variable we make the following cut:

• We accept only events where -25 cm <z-vertex<35 cm, to remove the background of events registered by the detector not origininating from collisions between the two particle beams (but for example from particles colliding with the beam pipe wall or with gas particles in the beam pipe).

In order to get a good M_x measurement, as much as possible of the diffractive system and as little as possible of the particles from proton dissociation should be included in the measurement. To make sure that the diffractive system is satisfactorily separated from the dissociated proton system and that the diffractive system particles has not gone into the beam pipe we make cuts:

• Only events including clusters having a maximum rapidity in the laboratory system $\eta_{max}<3$, and energy $E_{cluster}>400$ MeV are considered.

• Only events with energy in the forward plug calorimeter $E_{plug}<1$ GeV are accepted.

• The number of reconstructed muons in the three first layers (the other layers were broken 1994) of the forward muon detector (FMD) must be less then 2.

This combination of cuts, using information from calorimeter, plug and FMD is introduced to get an as complete coverage in θ-angle close to the beam pipe as possible. The calorimeter angular coverage is defined up to a rapidity of η=3.35 and the plug covers rapidities 3.54<η<5.1. The FMD is defined for 1.9<η<3.64. A particle colliding with some material (e.g. the beam pipe wall) produces a shower of secondary particles. Some of the secondaries may have large angles to the beam and may therefore be detected by the FMD. The FMD can thus be used to tag very high rapidity particles.

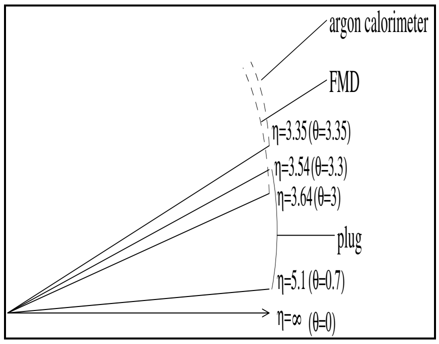

Figure 5.B: The angular coverage close to the beam pipe.

In our CONE algorithm (see chapter 4.4) jets are selected using the following cuts:

- The cone size is set to $\Delta R=1$

- A jet must have transverse momentum p_T >3.5 GeV in the hadronic CMS.

Only 2-jet events are then used for the calculation of $x_{parton/IP}$.

5.4 Resolutions, correlations and shifts

In this analysis, comparisons are made from detector to hadron level, rather than from detector to parton level, since the transition between parton and hadron level would require complex calculations, not defined in the current Monte Carlo generators. The resolution of a certain quantity on the detector level is defined as this quantity divided by the same quantity on the hadron level ("Q resolution" = "detector level Q" / "hadron level Q"). The division is made for all events giving a resolution distribution curve. A Gauss distribution is fitted to this curve. It should be peaked at 1, and if it is not, we conclude that there is a systematic error, a shift, in the detector level quantity compared to the hadron level. We correct shifts either by simply multiplying with a factor on the detector level, or first adding a constant to them and then multiplying by a factor. The mean deviation, σ, of the Gaussian fit will then be used as a measurement of the resolution.

To get an idea of how the quantity values on the detector and hadron level are related, so-called correlation plots are made. In the correlation plots we always have the hadron level quantity values on the x-axis and detector level values on the y-axis. A linear fit to such a plot should if there is no systematic shift be described by an x = y ("detector level Q" = "hadron level Q") line in the x-y plane. Shifts are in correlation plots observed as systematic deviations from this line.

In the following plots, events that are *not* 2-jet events on hadron level are cut away. This is done since $\hat{s}$ and $x_{parton/IP}$ are not defined on the hadron level for these events. (No other cuts are made on the hadron level)

5.5 Results

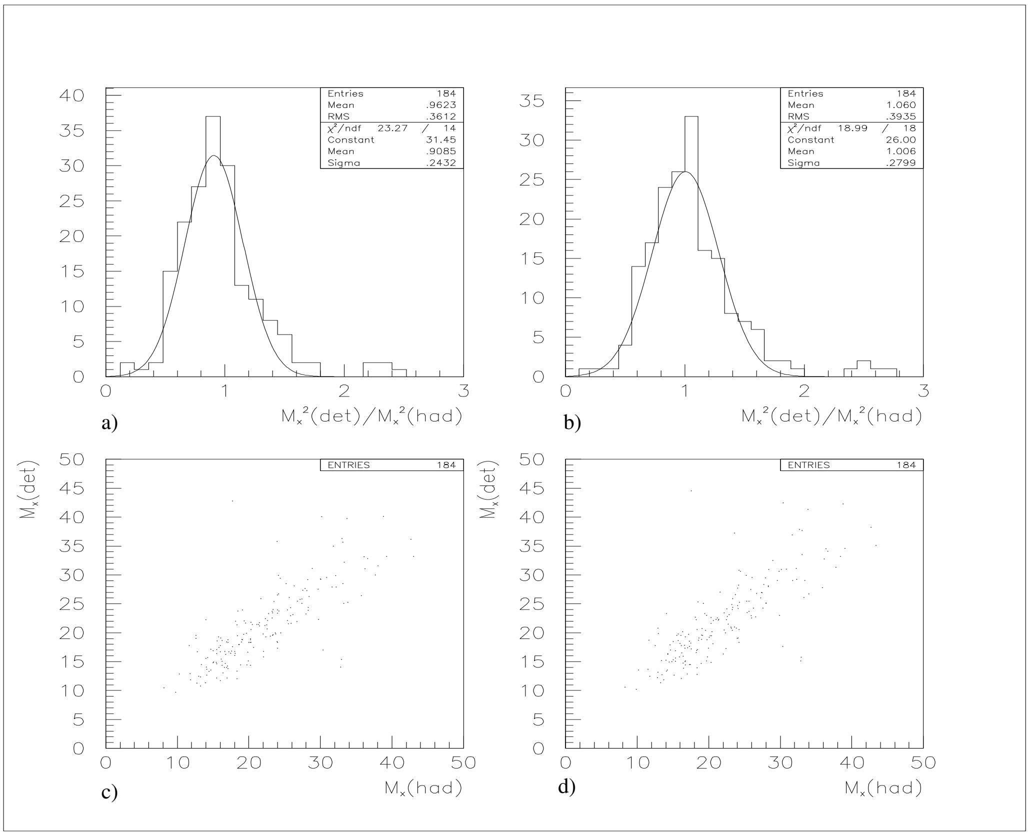

Figure 5.C: M_x resolution and correlation, shifted: a), c) and with the shift corrected: b), d).

The M_x resolution (M_x(det)/ M_x(had)) and correlation plots are shown in fig. 5.C. There is a shift in M_x, the Gauss fit having a mean of about 0.91 (see fig. 5.C.a) i.e. the detector level M_x that on average is approximately 9% smaller than the hadron level M_x. Some of the energy of the diffractive system thus seems to be lost due of detector effects. The shift is corrected using a multiplicative factor. M_x has a reasonable resolution, $\sigma \approx 0.28$ (for the Gauss fit with the shift corrected, fig. 5.C.b). The correlation is satisfactorily concentrated to the diagonal line $M_x(\text{det}) = M_x(\text{had})$ (as expected when σ is small) and the spread of the correlation line is approximately equally large over the whole M_x interval. The resolution is hence well defined, meaning it is close to the same value for all values of M_x.

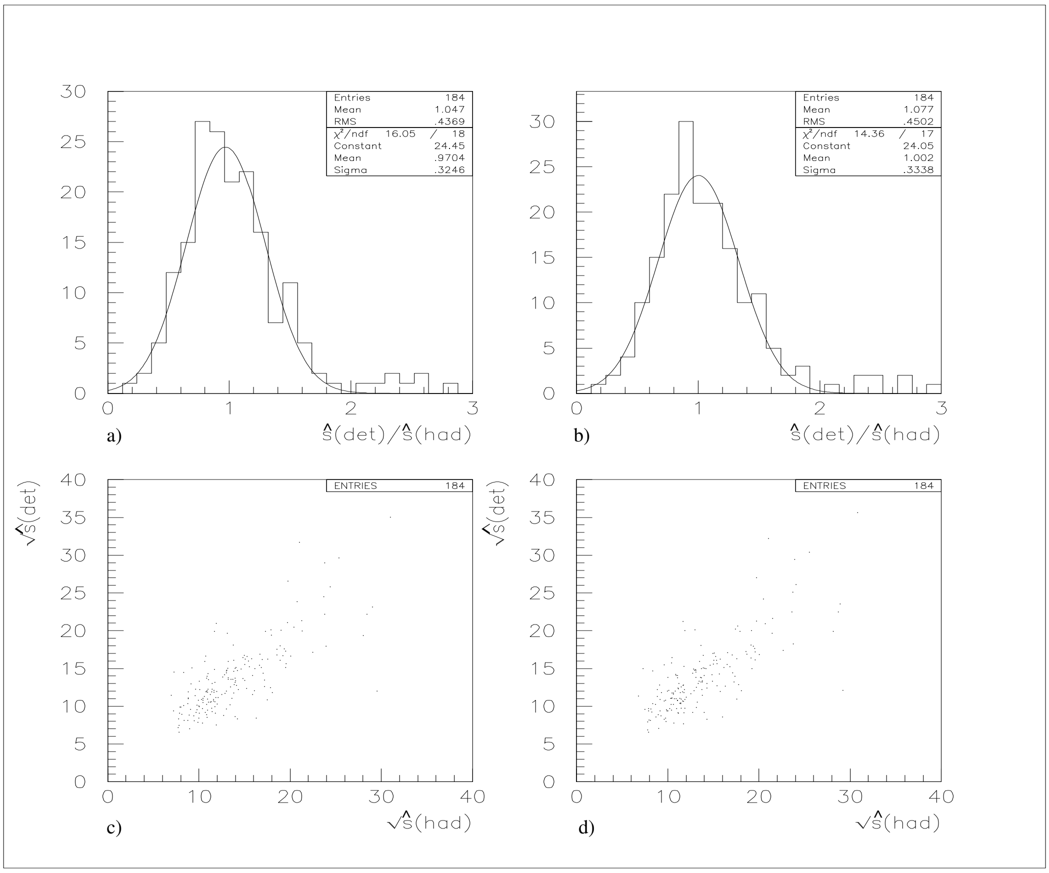

Figure 5.D: $\hat{s}$ resolution and correlation, shifted: a), c) and with the shift corrected: b), d).

The $\hat{s}$ resolution ($\hat{s}$(det)/$\hat{s}$(had)) and correlation plots are shown in fig. 5.D. There is a small shift in $\hat{s}$, approximately 3 % (fig. 5.D.a) The shift is corrected using a multiplicative factor. The resolution after the shift correction: $\sigma \approx 0.33$ (for the Gauss fit, fig. 5.D.b) is reasonable. The correlation plot also looks reasonable, the spread of the correlation is more or less equally large for all values of $\hat{s}$, meaning the resolution is well defined.

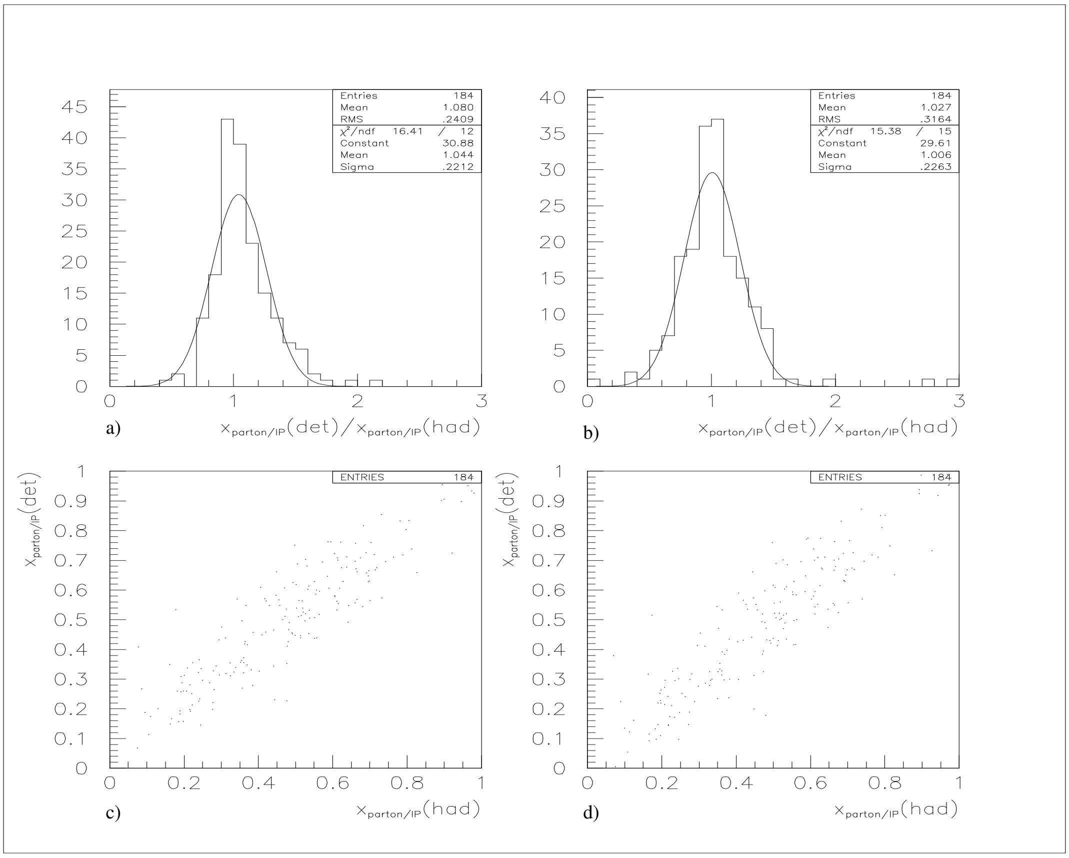

Figure 5.E: $x_{parton/IP}$ resolution and correlation, shifted: a), c) and with the shift corrected b), d).

The $x_{parton/IP}$ resolution and correlation plots can be seen in fig. 5.E. There is a small shift in the resolution (fig. 5.E.a) and the correlation line (fig. 5.E.c) seems to cross the y-axis above $y = x_{parton/IP}$ (det) = 0. The shift is therefore corrected using first an additive constant and then a multiplicative factor. ($x_{parton/IP}$ is calculated using the original M_x and $\hat{s}$, without first correcting their shifts. The shift in $x_{parton/IP}$ is then corrected.) The $x_{parton/IP}$ resolution is good, $\sigma \approx 0.23$ (for the Gauss fit of the plot with the shift corrected (5.E.b)), which is an even smaller σ than for the Gauss fits of both the M_x and $\hat{s}$ resolution plots. This indicates that a cancellation of systematic errors between these two variables takes place when they are used to calculate $x_{parton/IP}$ = $(Q^2 + \hat{s})/(Q^2 + M_x^2)$. With the shift corrected (fig. 5.E.d) the $x_{parton/IP}$ correlation line is well concentrated around the diagonal line, and the resolution is well defined.

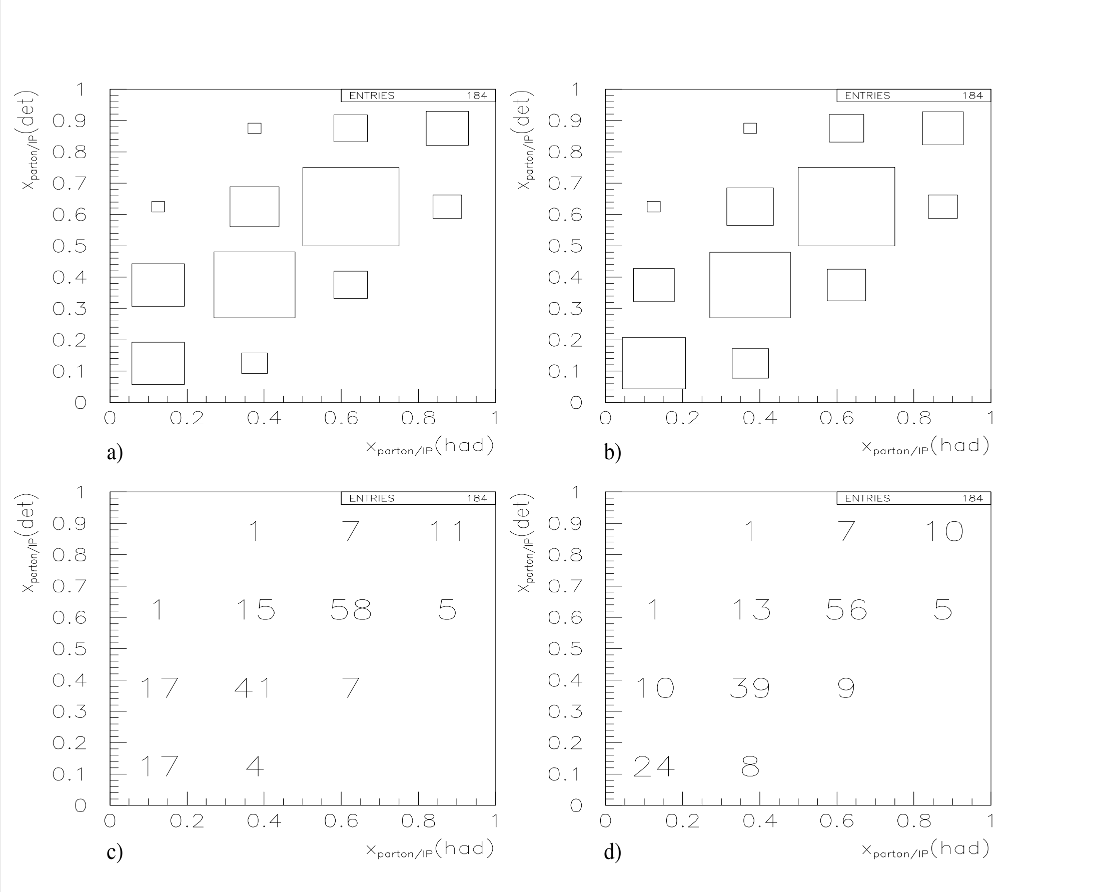

Figure 5.F: $x_{parton/IP}$ correlations, using for 4 bins. Plots are made using relatively sized boxes: a) shifted and b) with the shift corrected, and number of events: c) shifted and d) with the shift corrected.

Fig. 5.F again shows the $x_{parton/IP}$ correlations, now with the events divided up into 4 bins. Looking at these plots, we see that the shift correction improves the $x_{parton/IP}$ correlation. The correlation plot in which the shift is corrected (fig. 5.F.b) has a more symmetric shape than the plot of the original correlation (fig. 5.F.a). Also, if we look at the number of events (fig. 5.F.a and fig. 5.F.b) generated in the lowest $x_{parton/IP}$ bin on the hadron level axis, we see that some events that are reconstructed in higher bins on the detector level are "moved" by the shift correction into the lowest bin. (The shift correction only affects the detector level $x_{parton/IP}$ value, i.e. increasing or decreasing it and thus moving events up or down the detector level axis.)

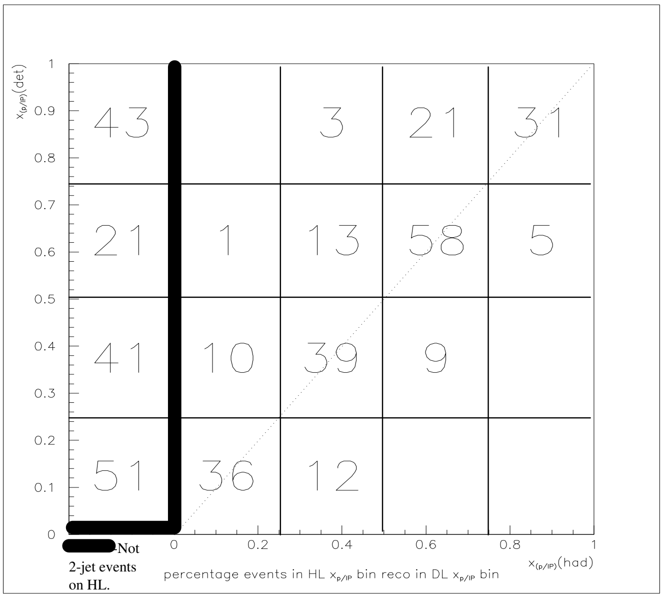

Figure 5.G: For each detector level bin, the percentage of events that was generated in a certain bin on hadron level.

In Fig. 5.G we have for each bin on the detector level (after the shift has been corrected) calculated the percentage of events that was generated in a certain bin on hadron level. The percentage of events in the diagonal bins is satisfactorily high. In the leftmost bin on the hadron level axis the percentage of events that are non 2-jets on hadron level, and for which $x_{parton/IP}$ is therefore undefined on the hadron level is displayed. Since this percentage of events is large, it requires further investigation.

The p_T spectrum of the jets is a steeply falling distribution. The resolution of the detector is limited i.e. the detector can never measure a quantity value perfectly, but will to some extent "smear" it out in an interval around the true value. When applying a sharp jet cut at 3.5 GeV on the detector level we may therefore accept jets that have p_T close to 3.5 on the hadron level. The p_T spectrum of the least energetic hard parton when the 2-jet cut on the detector level has been made is shown in fig. 5.H. We observe some QPM events (p_T =0 in the plot), but most of the first order events having a hard parton p_T <3.5 have a p_T close to 3.5. The p_T distribution is falling for p_T <3.5 (and not increasing as p_T approaches zero). This is what is expected from smearing effects. The events included in our $x_{parton/IP}$ measurement, accepted as 2-jet events on the detector level that are 1-jet events on the hadron level will therefore not affect the measurement to a large extent.

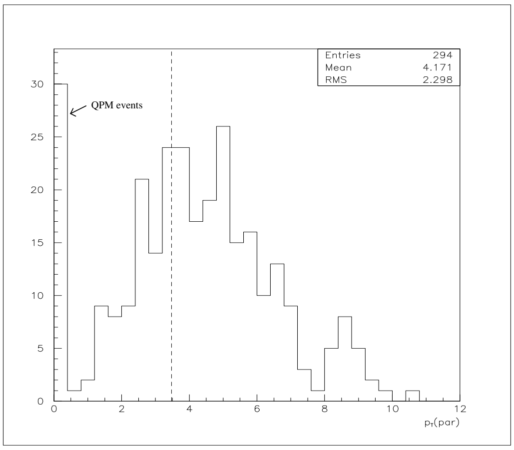

Figure 5.H: p_T of the least energetic hard parton for 2-jet events on detector level.

5.6 The $x_{parton/IP}$ distribution

Luminosity, L, is defined as being the number of collision events taking place per time and area-unit, L = $[(\mathrm{cm})^{-2}\ \mathrm{s}^{-1}]$. The cross-section of a certain process can be interpreted as the relative probability for it to occur. The number of events, N, of a process with the cross-section σ, expected to occur during a time interval $\Delta t = t_2 - t_1$ can be calculated as the integrated luminosity times the cross-section: $N = \int_{t_1}^{t_2} L \cdot dt \cdot \sigma$. The integrated luminosity is given in units of $(\mathrm{pb})^{-1}$ and the cross-section in (pb); 1b = 1barn = $10^{-24}\,(\mathrm{cm})^2$. The experimental data sample of diffractive events used in this study corresponds to an integrated luminosity of 1.96 $(\mathrm{pb})^{-1}$ and was collected with H1 during 1994. The simulated diffractive event sample corresponds to an integrated luminosity of 3.625 $(\mathrm{pb})^{-1}$.

A division of the $x_{parton/IP}$ distribution into 4 bins is made to get a reasonable amount of events per bin. The total number of events was 122 in the experimental plot (and 294 in the simulated plot). We normalise the $x_{parton/IP}$ distribution with the integrated luminosity and the bin-width to get the differential cross-section $d\sigma/d\,x_{parton/IP}$.

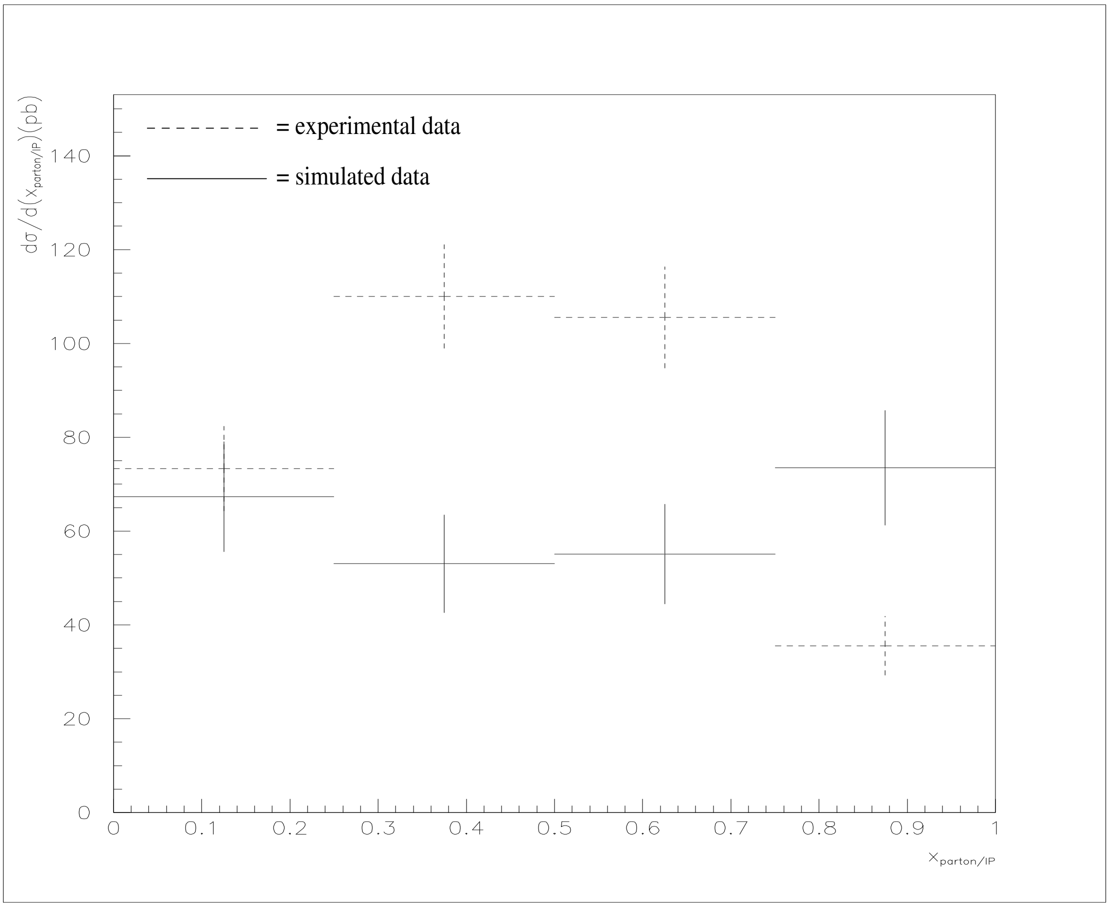

Figure 5.I: The $x_{parton/IP}$ differential cross-section ($d\sigma/d\,x_{parton/IP}$) retrieved from experimental data (line) and simulated data (dashed line).

The distribution is plotted in fig. 5.I, using error bars proportional to the square-root of the number of events in each bin, corresponding to the statistical error. The total cross-section of the experimental data is about 250 (pb) and of the simulated data about 325 (pb). The difference between the experimental and simulated distribution is only within the ranges of the error bars in two of the 4 bins. There also seems to be differences in the shape of the two distributions. These differences between experimental and simulated data could be an indication of the structure function used in the simulations not giving a correct description of the parton distribution. The F_2^D structure function is mainly sensitive to the quark content of the pomeron. On the other hand, the 2-jet sample obtained is strongly affected by the gluon distribution, via BGF. Looking at the experimental distribution we see that the cross-section of the top $x_{parton/IP}$ bin ($0.75 < x_{parton/IP} < 1$) is higher than the simulated distribution cross-section in this bin, even though the total simulated cross-section is larger than the total experimental cross-section. For events in which the 2-gluon exchange process takes place, we expect $x_{parton/IP}$ to be close to 1, since there is no pomeron remnant in this process. The high cross-section in the top $x_{parton/IP}$ bin could hence be an indication of the 2-gluon exchange process playing a part in diffractive e-p scattering.

Acknowledgements

I would like to thank the following persons:
Leif Jönsson and Hermann Küster for supervision and help.
Christian Jacobsson, Hannes Jung, Morten Nyberg-Werther and Joachim Stier for tutoring me.
Magnus Lindström for all the help.
Peer-Oliver Meyer and Markus Wobisch for the help with H1TOX.
Bertrand Laforge for providing DS information and Jürgen Spiekerman for the help with implementing combined objects.

References

• B.R Martin, G. Shaw, *Partilce Physics*, John Wiley & Sons, 1994
• Hans-Uno Bengtsson, Gösta Gustafson, Lena Gustafson, *Kvarken och universum*, Corona, 1994
• B.H Wiik, *Hera Status*, Physics at HERA vol. 1 (1991) 1
• ZEUS Collab., *Observation of Events with a Large Rapidity Gap in Deep Inelastic Scattering at HERA*, DESY 93-093
• I. Abt et al., H1 Collab., DESY 93-103
• H1 Collab., *Observation of hard proocesses in rapidity gap events in γp interactions at HERA*, Nucl. Phys. B 435 (1995) 3-20
• G. Wolf, *HERA physics*, DESY 94-022, Hamburg
• M. Bengtsson et al. *Parton Cascade Evolution and Events Structure at HERA*, Proc. of the HERA Workshop vol. 1 (1987) 149
• B. Andersson et al., Phys. Rep. 97 (1983) 31
• V. Hedberg et al. *Study of jet reconstruction algorithms from deep-inelastic events in γp interactions at HERA,* Z. Phys. C 63 (1994) 49
• G. Grindhammer, Monte Carlo Generators for ep Physics, at HERA vol. 3 (1991) 1153
• P. Bruni, G. Ingelman, A. Solano, *Diffractively Produced Hadronic Final States and the Pomeron Structure*, Physics at HERA vol. 1 (1991) 363
• G. Ingelman, K. Prytz, *The Pomeron structure in DIS and gluon recombination effects*, Z. Phys. C 63 (1994) 49
• H. Jung, *Hard diffractive scattering in high energy ep collisions and the Monte Carlo generator RAPGAP*, DESY 93-182, Hamburg
• UA8 Collab. R. Bonini et al. Phys. Lett. B 211 (1988) 634
• G. Ingelman, P.E. Schlein, *Jet Structure in High Mass Diffractive Scattering*, Phys. Lett. B 152 (1985) 681
• H1 Collab., *First Measurement of the deep-inelastic structure of proton diffraction*, Phys. Lett. B 348 (1995) 681
• H1 Collab., *A direct measurement of the Gluon Density in the Proton at Low x*, DESY 95-086
• A. Breakstone et al., Z. Phys. C48 (1990) 569, Z. phys. C58 (1993) 283
• B. A. Kniehl et al., *Diffractive Photoproduction of Jets with a Direct Pomeron Coupling at HERA*, DESY 94-140
• Morten Nyberg-Werther, *Studies of Various Aspects of the Proton Structure in Deep Inelastic Scattering at HERA and Identification of Quark and Gluon Jets*, Ph.D. Thesis, Lund University, 1994
• A. Mehta, *Measurement of the diffractive structure function and calibration of the FMD at H1*, University of Manchester
• H1 Collab., *Measurements of Jet Producitons and Energy Flow in Diffractive ep Interactions at HERA*, Paper pa02-062, Submitted to the 28th international Conference on High Energy Physics ICHEP', Warsaw, Poland, July 1996
• H1 Collab., *First Measurement of the Deep-Inelastic Structure of Proton Diffraction*, DESY 95-36

• H1 Collab., *A Measurement and QCD Analysis of the Diffractive Structure function* $F_2^{D(3)}$, Paper pa02-61 Submitted to the 28th International Conference in High Energy Physics ICHEP'96, Warsaw, Poland, July 1996

• J.Bartels et al., *Azimuthal Distribution of Quark-Antiquark Jets in DIS Diffractive Dissociation*, DESY 96-085